The Journal of Chemical Physics ARTICLE pubs.aip.org/aip/jcp

Acid-induced acceleration of kinetics and dynamics during thermal gelation of egg yolk

Cite as: J. Chem. Phys. 164, 135102 (2026); doi: 10.1063/5.0319351
Submitted: 23 December 2025 • Accepted: 16 March 2026 •
Published Online: 1 April 2026

Nimmi Das Anthuparambil,[1,2,a)] Sonja Timmermann,[1] Michelle Dargasz,[1] Sebastian Retzbach,[3] Maximilian D. Senft,[3] Fajun Zhang,[3] Michael Paulus,[4] Fabian Westermeier,[2] Michael Sprung,[2] Frank Schreiber,[3] and Christian Gutt[1,a)]

AFFILIATIONS

[1] Department Physik, Universität Siegen, 57072 Siegen, Germany
[2] Deutsches Elektronen-Synchrotron DESY, 22607 Hamburg, Germany
[3] Institut für Angewandte Physik, Universität Tübingen, 72076 Tübingen, Germany
[4] Fakultät Physik/DELTA, Technische Universität Dortmund, 44221 Dortmund, Germany

[a)] **Authors to whom correspondence should be addressed:** nimmi.anthuparambil@uni-siegen.de and christian.gutt@uni-siegen.de

ABSTRACT

The effect of lowered pH on the thermal gelation behavior of hen egg yolk was investigated over the temperature range of 58–72 °C using low-dose X-ray photon correlation spectroscopy in ultra-small-angle X-ray scattering geometry. Progressive structural and dynamical alterations were observed at room temperature with decreasing pH, indicative of acid-induced protein denaturation, which correlates with an increase in yolk viscosity. Temperature- and pH-dependent structural and dynamic investigation suggests an acceleration in gel formation with decreasing pH. The time–temperature superposition relationship observed in all samples suggests an identical mechanism underlying protein aggregation–gelation with a temperature-dependent reaction rate. The sol–gel transition time extracted from kinetic and dynamic information follows Arrhenius behavior, with no significant change in the activation energy (450 ± 20 kJ/mol) of gelation. However, the prefactor A systematically decreases with decreasing pH, indicating that acidification accelerates gelation primarily by increasing the frequency of productive encounters without altering the fundamental energy barrier of the process.

I. INTRODUCTION

Protein gelation is a complex physicochemical process in which proteins undergo structural rearrangements and intermolecular association to form a three-dimensional network capable of immobilizing water and other solutes. The process encompasses multiple length and time scales,[1–9] from molecular conformational transitions to mesoscale network formation, and it is influenced by non-covalent interactions such as hydrophobic forces, hydrogen bonding, and electrostatics. Additives such as salts,[5,7,9–11] acids,[12–15] alkali,[16,17] and others[18,19] can significantly alter the gelation pathway by modulating protein conformation, intermolecular interactions, and the surrounding solvent environment. From a physicochemical standpoint, these components influence key factors such as protein charge distribution, hydration shell dynamics, and the balance between attractive and repulsive forces, thereby affecting both the kinetics and thermodynamics of network formation. Additives may promote or inhibit gelation, modify the microstructure, or induce transitions between different gelation regimes (e.g., from diffusion-limited to reaction-limited aggregation). A detailed understanding of how additives modulate the gelation pathway—by influencing protein–protein and protein–solvent interactions—is essential for elucidating the fundamental mechanisms of gelation and for tailoring gel properties to suit specific applications in food,[20–22] biomedical,[23,24] and biotechnology.[25,26]

Egg yolk, due to its rich and diverse composition of proteins and lipids, serves as a multifunctional ingredient widely employed in food systems,[27,28] biotechnology,[21,29] and other applications.[21] It

exhibits complex phase behavior and gelation characteristics, with functional properties including emulsification, foaming, coagulation, and thermal gelation.[5,21,30,31] Citric acid, a naturally occurring organic acid, is frequently used to adjust the pH and ionic environment of protein-rich systems, including egg yolk. By lowering the pH, citric acid induces conformational changes in yolk proteins and influences their charge distribution and intermolecular interactions. These alterations can significantly affect the gelation kinetics and network structure formed during thermal processing. Moreover, citric acid's chelating properties and antimicrobial activity provide additional functional benefits, enhancing product safety and shelf life. For example, the growth of *Clostridium botulinum* bacteria is strongly inhibited as pH decreases from near-neutral (≈7.0) to 4.6, resulting in a reduction in bacterial numbers by a factor of 1×10^6 (six-log reduction) and establishing pH 4.6 as a critical safety threshold.[32] In acidified egg yolk systems, while pH 3.9 still permits *Salmonella* bacteria growth at 25 °C, lowering the pH to 2.9 leads to over a 10 000-fold reduction (four-log) within 24 h, demonstrating effective bacterial inactivation.[33] However, strong acidification (pH < 4) often results in an undesirable sour taste in foods. To balance safety and sensory quality, producers typically use milder acid levels (pH > 4) combined with other preservation methods—such as refrigeration, thermal processing, and preservatives—rather than relying solely on low pH. This combination of preservation techniques allows food safety to be maintained across a wider range of pH values, which motivates our study over a pH range of 2.9–6. Despite the widespread use of citric acid, a detailed understanding of its effects on yolk gelation microstructure and dynamics remains limited.

Previous studies have primarily relied on rheological measurements[5,13,14,34,35] and microscopy techniques[13,34,35] to examine how additives, such as acids and salts, affect the viscoelastic properties and microstructure of protein-based gels. While these approaches have provided valuable macroscopic insights, they offer limited information about the underlying structural and dynamical processes occurring at the level of individual yolk components during thermal gelation. This limitation is critical, as protein denaturation and aggregation occur over a broad range of length scales, from nanometers to micrometers, and evolve over large time scales as well. The inherent heterogeneity of yolk, composed of a mixture of proteins and fat, further complicates conventional analysis, making it challenging to capture the full picture of gelation dynamics. More generally, the relaxation modes of proteins in solution provide an important framework for interpreting molecular behavior in complex food matrices.[2,4,36]

To overcome these challenges, we utilize low-dose X-ray photon correlation spectroscopy (XPCS), a technique uniquely suited to probe both the structure and dynamics of soft and hard condensed matter systems *in situ* during thermal processing. XPCS has been extensively employed to investigate the relaxation behavior of proteins,[6,8,9,37–41] as well as other complex systems, including polymers,[42–44] colloids,[45] glasses,[46] and a variety of soft and hard materials.[47,48] In our previous work, we applied XPCS to elucidate the role of ionic strength in modulating yolk gelation kinetics, revealing that salt addition can significantly delay gel formation.[7] In the present work, we extend this approach to examine how acidification, through pH reduction, modifies the nanoscale dynamics and structural evolution during thermal gelation, offering new insights into the fundamental mechanisms governing protein–lipid interactions in complex food systems.

We investigate the effect of citric-acid-induced pH reduction on the thermal gelation of egg yolk using X-ray photon correlation spectroscopy (XPCS) in an ultra-small-angle X-ray scattering (USAXS) geometry. By simultaneously probing the structural evolution and microscopic dynamics during heating, we examine how acidification influences protein denaturation, aggregation, and gel formation across a broad range of length and time scales. By analyzing the structural and dynamic changes, we estimate the sol–gel transition time, which indicates the transition point from the protein denaturation–aggregation-dominated phase to protein gel formation. Furthermore, we analyze the temperature dependence of the sol–gel transition time to assess whether changes in pH modify the apparent activation energy or instead affect the kinetic prefactor governing gelation. This approach provides a framework for understanding the effect of additives on protein gelation by simultaneously following the changes in kinetics and dynamics.

II. EXPERIMENTAL

A. Sample details

The egg yolk used in this study was obtained from a hen egg purchased at a local supermarket. The extraction procedure involved three steps. First, the yolk was separated from the egg white using a steel strainer and rinsed with Milli-Q water to remove residual albumen. Second, the cleaned yolk was placed on filter paper and gently rolled several times to absorb excess water and albumen from its surface. Third, the vitelline membrane was pierced with a plastic pipette tip to release the yolk, which was then collected and stored in a 15 ml Falcon tube at 5 °C.

Anhydrous citric acid was purchased from Sigma-Aldrich, and 0.6, 0.8, 1, 2, 3, 4, and 5 M solutions were prepared. To 2 g of yolk, 70 μl of citric acid solution was added and mixed with a magnetic stirrer for ≈6 h. The weight percent of citric acid in the final mixture is given in Table I (see supplementary material for calculations). The mixed samples were stored in a freezer at 5 °C for the duration of the experiment. The pH value of the solution was estimated using a pH meter (METTLER TOLEDO LLC, US) and is given in Table I.

B. Coherent X-ray scattering experiments

Low-dose USAXS-XPCS measurements in transmission geometry[6] were performed at the beamline P10 of PETRA III, DESY, Hamburg, Germany. A schematic representation of the experimental setup is shown in Fig. 1. An X-ray beam with a photon energy of 8.54 keV and a beam size of 100 × 100 μm^2 was directed onto the samples, which were loaded into 1.5 mm (diameter) quartz capillaries, sealed with Parafilm, and mounted within a Linkam heating stage (Linkam Scientific Instruments Ltd., UK) for USAXS–XPCS measurements, as illustrated in Fig. 1. X-rays scattered from the sample were recorded using an EIGER X4M area detector positioned 21.2 m downstream from the sample. The detector has a pixel size of 75 × 75 μm^2 and an active area of 155.2 × 162.5 mm^2. This configuration enabled access to a momentum transfer (q) range of 0.005–0.22 nm^{-1}.

The yolk samples were heated to temperatures ranging from 58 to 72 °C. Heating was performed from room temperature (22 °C) to

TABLE I. Overview of sample names and respective citric acid concentrations and pH.

Sample	Amount of yolk[a] (g)	Molarity of added citric acid (mM)	Amount of citric acid added (μl)	Citric acid in the final mixture[b] (w/w%)	pH of sample
Yolk	2	...	70	0	5.94
y600	2	600	70	0.39	5.14
y800	2	800	70	0.52	5
y1000	2	1000	70	0.65	4.83
y2000	2	2000	70	1.3	4.27
y3000	2	3000	70	1.95	3.98
y4000	2	4000	70	2.6	3.77
y5000	2	5000	70	3.25	2.92

[a]Water content in yolk is ≈52%.
[b]See supplementary material for calculations.

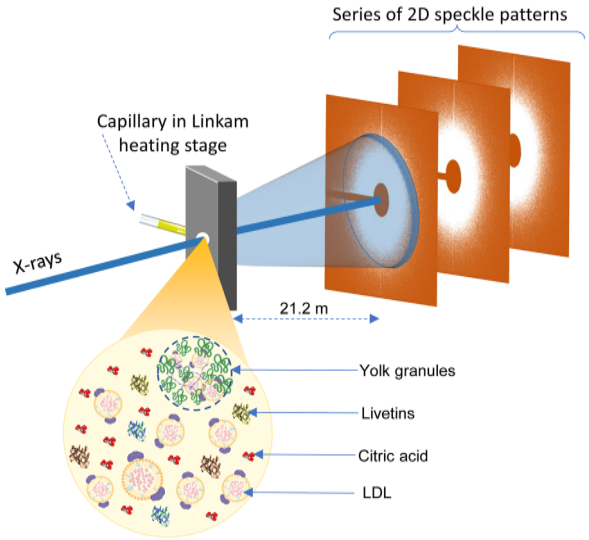

FIG. 1. Coherent X-rays from a synchrotron radiation source are scattered by the egg yolk sample contained within a quartz-glass capillary. A two-dimensional detector positioned 21.2 m downstream from the sample collects a series of speckle patterns for analysis. The schematic below the sample position illustrates the various components of egg yolk with citric acid. Egg yolk is composed of ~52% water, with the remaining dry matter primarily consisting of low-density lipoproteins (LDLs), yolk granules, and a range of proteins known as livetins.[30] LDLs represent about 66% of the total dry matter. LDLs are core–shell nanoparticles with an average diameter of 30 nm.[21,30,49] The LDL core contains lipids such as triglycerides, cholesterol esters, and free cholesterol, which are encapsulated by a shell comprising phospholipids, cholesterol, and apolipoproteins.[21] Yolk granules account for ~22% of the dry matter and are spherical complexes ranging from 0.3 to 2 μm in diameter,[50–52] composed of LDLs, high-density lipoproteins (HDLs), and the protein phosvitin.[53,54] Portions of this schematic were created using BioRender.

the target temperature at a constant ramp rate of 150 °C/min. Temperature calibration data for the Linkam heating stage are provided in the supplementary material. The time required to heat from 22 °C to the set temperature is denoted as $t_{heating}$. Throughout the text, two time scales are used: the isothermal waiting time, t_w, and the absolute waiting time, t'_w, which are related by $t_w = t'_w - t_{heating}$. Here, $t'_w = 0$ s marks the onset of heating.

Recent studies have shown that prolonged exposure to X-rays can induce radiation damage in protein samples, affecting both their structure and dynamics.[37,55–57] To mitigate such damage during measurements, we employed a protocol involving lateral translation of the capillaries by 200 μm between successive XPCS measurements, ensuring that each scan probed a fresh region of the sample. In addition, a carefully optimized combination of silicon absorbers was used to attenuate the beam, and the total exposure duration was strictly controlled to minimize radiation dosage. All experiments were conducted using low dose rates of 0.024 kGy/s, with the absorbed dose per scan kept below 5 kGy (see supplementary material for details). Data reduction and analysis were carried out using the Python-based package Xana[58] and the MATLAB-based XPCSGUI toolkit provided by beamline P10.

Time-resolved dynamics of the yolk system were analyzed through two-time correlation functions (TTCs),[8,47,59–61] defined as

$$C(q,t_1,t_2) = \frac{\langle I_{pixel}(q,t_1) I_{pixel}(q,t_2)\rangle}{\langle I_{pixel}(q,t_1)\rangle \langle I_{pixel}(q,t_2)\rangle}, \quad (1)$$

where I_{pixel} is the intensity at a pixel, $\langle \ldots \rangle$ denotes the average over pixels in a q-range of $q \pm \delta q$, and t_1 and t_2 are different experimental times. Here, the scattering wavevector q is given by $(4\pi/\lambda)\sin(\theta)$, where 2θ is the scattering angle and λ is the incident X-ray wavelength. In the TTC maps, the absolute waiting time, t'_w, progresses along the diagonal ($t_1 = t_2$), with $t'_w = 0$ s corresponding to the onset of heating. The relative lag time $t = |t_1 - t_2|$ is represented along the off-diagonal direction.

The evolution of sample dynamics at different stages of gelation is captured by extracting one-time autocorrelation functions, $g_2(q,t,t'_w)$, from the TTC map via diagonal slices along constant absolute waiting times,[59,62] as depicted in Fig. 6(a). These autocorrelation functions quantify the temporal decay of intensity fluctuations at each wavevector and provide an estimate of dynamic relaxation in the system. To characterize the relaxation behavior, the functions are modeled using a stretched exponential form derived from the intermediate scattering function (ISF),[63]

$$g_2(q,t,t'_w) = 1 + \beta\,|f(q,t)|^2 = 1 + \beta\,|\exp\left[-(t/\tau)^{\gamma}\right]|^2, \qquad (2)$$

where $f(q,t)$ is the intermediate scattering function, τ is the characteristic relaxation time, β is the experimental speckle contrast, and γ is the Kohlrausch–Williams–Watts (KWW) exponent[64] describing the width of the relaxation spectra.

Here, the exponent γ characterizes the shape of the intensity autocorrelation function g_2 and provides insight into the nature of the underlying dynamics. A purely exponential decay ($\gamma = 1$), together with a relaxation time scaling as $\tau(q) \propto q^{-2}$, is characteristic of Brownian diffusion. Deviations from this behavior are commonly observed in complex and soft matter systems. In particular, compressed exponential decays ($\gamma > 1$) are typically associated with arrested or out-of-equilibrium states, such as gels, foams, and glasses,[65–67] as well as with stress-driven dynamics in solid-state systems.[68] Conversely, stretched exponential decays ($\gamma < 1$) can arise from several mechanisms, including memory effects associated with transient caging,[41,69] dynamical heterogeneity that may arise from polydispersity, spatially heterogeneous relaxation, or the coexistence of regions with different dynamical timescales within the sample.[65]

III. RESULTS AND DISCUSSION

A. Effect of decreasing pH on egg yolk microstructure and dynamics at room temperature

Figure 2(a) shows the scattering intensity profile, $I(q)$, for native egg yolk (black curve). At low q, the intensity follows a q^{-4} dependence, characteristic of Porod scattering from the interfaces of spherical yolk granules. A distinct structure factor peak appears at $q \approx 0.22$ nm^{-1}, corresponding to the spatial correlations among low-density lipoprotein (LDL) particles.[6] The introduction of citric acid leads to subtle but noticeable modifications in the $I(q)$ profiles, suggesting acid-induced alterations in the yolk microstructure. Note that the pH of native egg yolk is roughly 6, and upon addition of citric acid at different molarities, the pH decreases, as illustrated in Table I. The weight percent of citric acid in the final mixture is given in Table I (see supplementary material for calculations).

To relate the experimental acidification level to common culinary practice, the amount of citric acid used in our model system can be expressed in kitchen-relevant terms. In the y600 sample, 70 μl of a 600 mM citric acid solution was added to 2.0 g of egg yolk. Scaled to a whole egg yolk (≈18 g), this corresponds to ≈73 mg of citric acid, which is equivalent to ≈1.5 ml of fresh lemon juice (see supplementary material for calculations). This volume is roughly 30 drops (1 drop ≈ 0.05 ml) or about 0.3 teaspoon, making the acidification level comparable to adding a small splash of lemon juice during cooking.

Upon lowering the pH, a new power-law regime appears in the q-range 0.02–0.2 nm^{-1}. To quantify this behavior, we fit the scattering intensity $I(q)$ in two regions: a low-q range (0.0135–0.02 nm^{-1}) and a higher-q range (0.04–0.07 nm^{-1}). The data are fitted using power-law functions of the form $I(q) \propto q^{p_1}$ and $I(q) \propto q^{p_2}$ for the low- and high-q regions, respectively. The resulting exponents are shown in Fig. 2(b). The Porod exponent p_1 remains nearly constant down to pH ≈ 3.7, with a slight increase observed only at the lowest pH of 2.92. This minimal variation suggests that the spherical structure of the granules remains largely stable against acidification above a pH of 3.7. On the other hand, the power-law exponent p_2

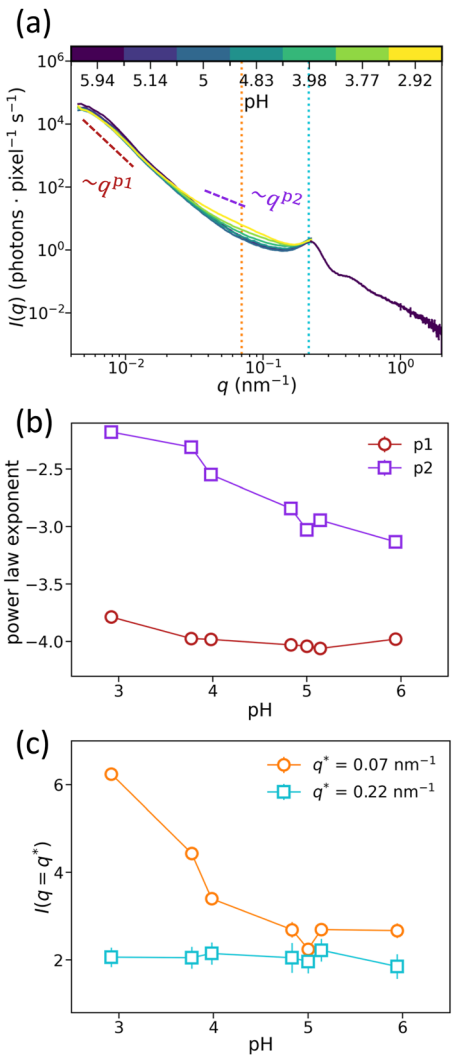

FIG. 2. (a) Representative scattering intensity curves of egg yolk at different pH values, as mentioned in the color scale, with intensity normalized to full-beam conditions (attenuation-corrected) and reported as photons per pixel per second. $I(q)$ follows $I(q) \propto q^{p_1}$ and $I(q) \propto q^{p_2}$ at lower and higher q values, respectively, which are indicated using dashed lines. The orange and blue vertical dotted lines indicate the q values 0.07 and 0.22 nm^{-1}, respectively. (b) Variation of the power-law exponents p_1 and p_2 with pH, illustrating the influence of acidification on gelation dynamics. (c) $I(q)$ at $q = 0.07$ nm^{-1} and $q = 0.22$ nm^{-1} as a function of pH.

continuously increases with decreasing pH from 5.94 (native egg yolk). Along with a change in p_2, the scattering intensity increases in the q-regime 0.02–0.2 nm^{-1} [Fig. 2(c)], indicating the formation of new structures. Furthermore, the addition of acid appears to have little effect on the overall spherical morphology of LDL particles, as indicated by the nearly unchanged scattering intensity near the structure factor peak at $q = 0.22$ nm^{-1} [Fig. 2(c) and Fig. S4 of the manuscript]. From these observations, we conclude that citric acid mainly affects the yolk proteins, and the increase in intensity

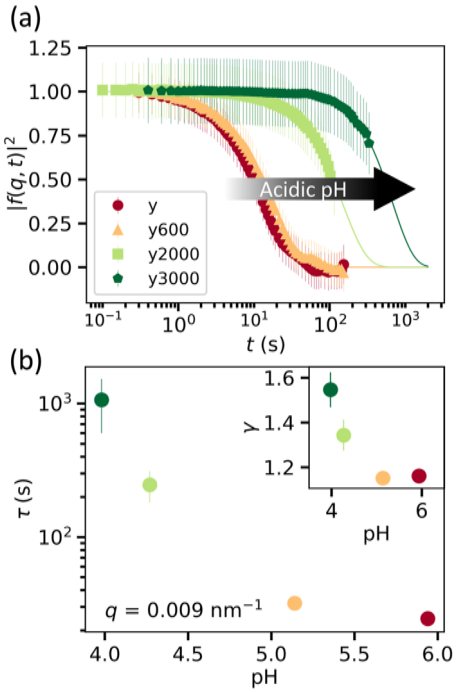

FIG. 3. (a) $|f(q,t)|^2$ of different samples at room temperature at $q = 0.009$ nm^{-1}. The solid lines are fits using Eq. (2). (b) The extracted τ as a function of pH. The inset shows the extracted γ as a function of pH.

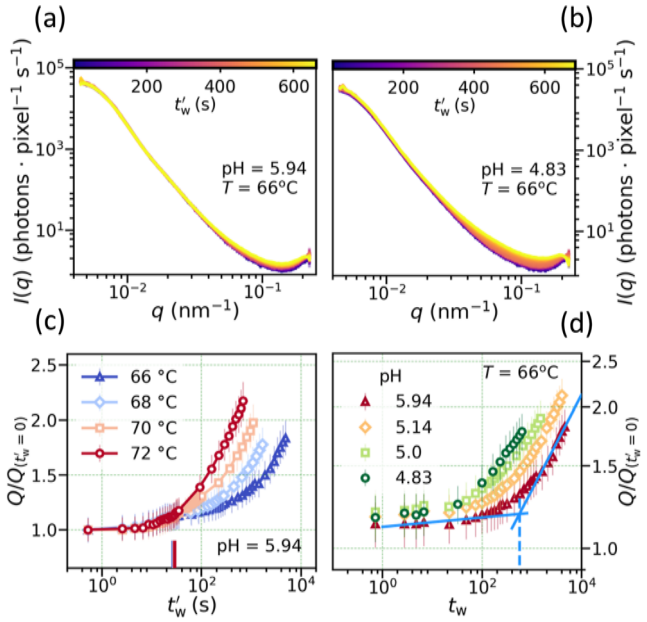

FIG. 4. Evolution of $I(q)$ of (a) pure egg yolk (pH = 5.94) and (b) y1000 (pH = 4.83) at $T = 66$ °C. Intensity is normalized to full-beam conditions (attenuation-corrected) and reported as photons per pixel per second. The color bar represents the absolute waiting time t'_w measured from the onset of heating at 22 °C. (c) The normalized scattering invariant $Q/Q_{(t'_w=0)}$ as a function of t'_w for yolk. Short vertical ticks along the horizontal axis denote $t_{heating}$ (time taken to reach the set temperature from 22 °C). The color of these lines matches that of the data points at the same temperature. (d) The log–log plot of the normalized scattering invariant $Q/Q_{(t'_w=0)}$ as a function of isothermal waiting time t_w for all samples at $T = 66$ °C. The blue curves indicate the power-law fits at low-t_w and high-t_w regions on pure yolk data (pH = 5.94), and the vertical dashed line indicates the intersection (t^*) of these power-law fits.

in the q-regime 0.02–0.2 nm^{-1} is comparable to that expected for temperature-induced denaturation of yolk proteins.[6]

Next, we examine the changes in the collective dynamics of egg yolk at room temperature as a function of decreasing pH. The intermediate scattering functions of yolk samples without and with added citric acid are compared in Fig. 3(a). A pronounced slowdown in dynamics is observed at lower pH values. To quantify this behavior, the ISFs are fitted using Eq. (2), and the extracted relaxation times are presented in Fig. 3(b). Overall, the results reveal an exponential slowdown of the dynamics with decreasing pH. The KWW exponent γ increases as pH decreases, indicating increasingly compressed relaxation spectra. The q-dependence of the relaxation times remains largely similar, as shown in Fig. S6.

B. Thermal gelation kinetics of yolk in acidified environments

Due to the high viscosity of samples at pH values below 4, capturing their slow dynamics with XPCS requires extended measurement times [see Fig. 3(b)]. To enable systematic exploration across multiple conditions and temperatures, we focused our temperature-induced gelation studies on a representative subset: y, y600, y800, and y1000, where the numbers correspond to the molarity of the citric acid solution added (see Table I for details).

Figure 4(a) shows representative $I(q)$ profiles during the thermal gelation of pure egg yolk at 66 °C. A pronounced increase in scattering intensity for $q > 0.02$ nm^{-1} indicates the denaturation of yolk-plasma proteins.[6] In contrast, the low-q region ($q < 0.02$ nm^{-1}) remains largely unchanged, suggesting that yolk granules retain structural stability at this temperature. However, when citric acid is introduced [Fig. 4(b)], a pronounced increase in $I(q)$ for $q > 0.02$ nm^{-1} is observed in comparison to the pure yolk case, highlighting enhanced protein denaturation under acidic conditions. To quantify the rate of structural evolution, we compute the scattering invariant[6–8] using the following relation:

$$Q = \int_{q_1}^{q_2} q^2\, I(q)\, \mathrm{d}q. \tag{3}$$

The scattering invariant was calculated by integrating the intensity over the range $q_1 = 0.02$ nm^{-1} and $q_2 = 0.17$ nm^{-1} as an increase in scattering intensity is observed in this q regime during heating. The resulting Q values, normalized to the initial state $Q(t'_w = 0\,\mathrm{s})$, are plotted in Fig. 4(c) and Fig. S5. Across all cases, several consistent trends emerge: (i) Q increases with time at every temperature, and (ii) once the target temperature is reached, the rate of increase in Q becomes strongly temperature-dependent, accelerating with higher temperatures. In Fig. 4(d), we present a comparison of $Q/Q(t'_w = 0)$ for all samples at $T = 66$ °C. It is evident that, at a fixed temperature

and isothermal waiting time, a decrease in pH leads to an increase in Q.

In addition, for each temperature, the slope of Q increases with t'_w after $t_{heating}$ [Fig. 4(c) and Fig. S5]. To characterize these changes, the data were fitted using a power-law function $Q/Q(t'_w = 0) \sim t'^{\alpha}_w$ at both low and high values of t_w [see fits on pH = 5.94 in Fig. 4(d)], where $t_w = t'_w - t_{heating}$ is the isothermal waiting time.

The presence of two distinct power-law regimes in the temporal evolution of the scattering invariant Q indicates a crossover between two dominant structural processes. The early-time regime, characterized by a relatively small power-law exponent, suggests the onset of yolk protein denaturation, consistent with the known denaturation of egg-yolk protein γ-livetins at $T > 60$ °C.[70] In general, when proteins are denatured, protein chains can interact more extensively through disulfide bonds, which leads to the formation of aggregates.[71,72] At later times, a second power-law regime with a markedly larger exponent emerges, signifying a rapid acceleration of structural rearrangements and suggesting the association and organization of these aggregates into an interconnected three-dimensional gel network.[5] The characteristic time t^*, defined by the intersection of the two power-law fits, therefore marks the transition from a denaturation-aggregation-dominated regime to a gelation-dominated regime and is identified as the sol–gel transition time. In addition, we observe structural changes at nanometer length scales (Fig. S8), with their growth markedly accelerated at lower pH (Fig. S9), aligning with the observations in Fig. 4(d).

Notably, when the time axis is normalized by the characteristic sol–gel transition time t^*, master curves emerge, as shown in Fig. 5. This observation reveals the presence of time–temperature superposition (TTS) behavior in the structural evolution during yolk gelation, indicating that a common underlying mechanism governs these changes across all samples, with the reaction rate modulated by temperature. As the pH drops below 5, the power-law exponent in the low-t_w region exhibits a modest increase, while the exponent in the high-t_w region shows a slight decrease (refer to the exponents presented in Fig. 5). This trend demonstrates that increasing acid concentration impacts the kinetics of structural evolution during heat-induced gelation. The importance of t^* is further highlighted when correlating this kinetic insight with dynamic measurements discussed in Sec. III C, providing a deeper understanding of the gelation process.

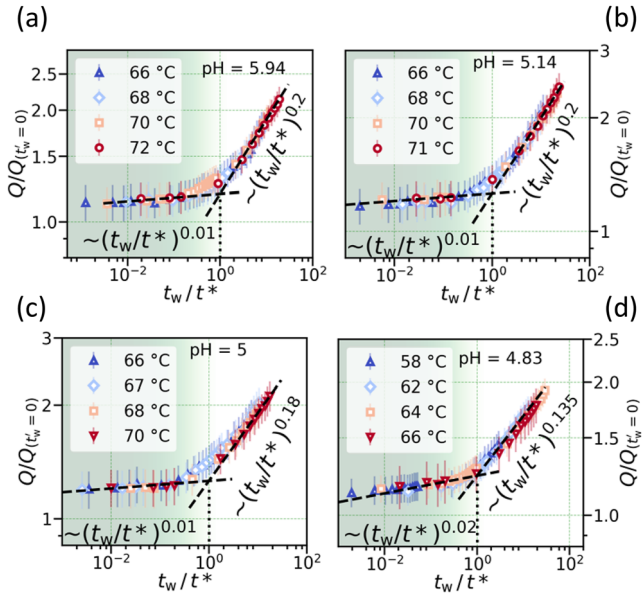

FIG. 5. The normalized scattering invariant $Q/Q_{(t'_w=0)}$ as a function of normalized isothermal waiting time t_w/t^* for (a) yolk, (b) y600, (c) y800, and (d) y1000. The dashed lines represent the power-law fits, with their corresponding exponents displayed alongside. In (a) and (b), the power-law exponents at low-t_w and high-t_w regimes are ≈0.01 and ≈0.2, respectively. In (c), the power-law exponents at low-t_w and high-t_w regimes are ≈0.01 and ≈0.18, respectively. In (d), the power-law exponents at low-t_w and high-t_w regimes are ≈0.02 and ≈0.135, respectively.

Reported isoelectric point values for the major protein components of hen egg yolk vary across the literature, reflecting its compositional complexity. Previous studies have placed the isoelectric point of yolk proteins in the acidic regime, with reported values ranging from approximately pH 5–6[73] and a pH of ≈4.6.[74] Despite this variability, both reports indicate that charge neutrality is approached at moderately acidic pH, where electrostatic repulsion between proteins is minimized. Approaching this regime is, therefore, expected to enhance aggregation propensity and promote protein–protein interactions, which is consistent with the observed acceleration of gel formation at lower pH in the present study.

C. Microscopic dynamics of thermal gelation of egg yolk at acidic pH

In this section, we investigate how citric acid influences the microscopic dynamics of egg yolk during thermal gelation. This is realized by calculating TTC maps using Eq. (1). Representative

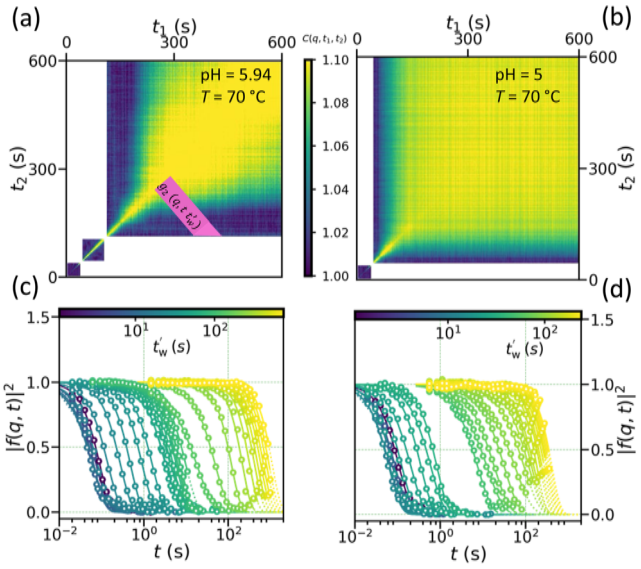

FIG. 6. TTC map of (a) yolk (pH = 5.94) and (b) y800 (pH = 5) during thermal gelation at T = 70 °C and q = 0.0055 nm^{-1}. For better visibility, individual TTCs are shown separately in Fig. S7 of the supplementary material. The corresponding intermediate scattering function of (c) yolk and (d) y800 heated to 70 °C as a function of absolute waiting times is denoted by the color bar.

TTC maps of the yolk and y800 sample heated to 70 °C are given in Figs. 6(a) and 6(b). There are three TTC maps in Fig. 6(a) (for better visibility, individual TTCs are shown separately in Fig. S7 of the supplementary material). Each of them is acquired from a fresh sample region along the capillary. The consistent and continuous dynamics observed across neighboring TTCs indicate that the X-ray beam had no noticeable impact on the sample behavior during measurements. The width of the yellow diagonal band in the TTCs is directly proportional to the relaxation time of the sample. The exponential increase in the width of this yellow band with increasing waiting time indicates an exponential increase in relaxation time and, hence, gel formation.[6] A comparison between Figs. 6(a) and 6(b) reveals that gel formation proceeds significantly more rapidly under acidic conditions.

To quantify these observations, we extract one-time correlation functions $g_2(q, t, t'_w)$ by slicing the TTCs diagonally into several sections. One such diagonal slice is illustrated in Fig. 6(a). These cuts are known as "constant sample age" cuts,[59,62] which are used for further analysis. The intermediate scattering functions, extracted from TTCs at various t'_w for yolk and y800 samples, are presented in Figs. 6(c) and 6(d), respectively. Here, solid lines represent fits using Eq. (2). The extracted relaxation times, τ, from the fits (at $q = 0.0055$ nm^{-1}), are plotted in Figs. 7(a)–7(d) for all samples and several temperatures. During thermal gelation of egg yolk, the temporal evolution of τ exhibits four distinct regimes (A, B, C, and D), as reported in our earlier work.[6] In this study, we focus on dynamics up to regime C due to experimental time constraints.

Regimes A and B are highlighted by a dotted circle and a green-shaded region in Figs. 7(a)–7(d). The relaxation times τ are extracted at a wavevector $q = 0.0055$ nm^{-1}, which corresponds to probing dynamics on a real-space length scale of ~1 μm ($2\pi/q$). This length scale is comparable to the size of yolk granules, which are micrometer-sized structural entities, and is much larger than the characteristic sizes of individual proteins and low-density lipoproteins, which are on the order of tens of nanometers. As a result, the measured dynamics primarily reflect the motion of yolk granules rather than that of smaller molecular components. Consistently, the low-q scattering is governed by a Porod power-law behavior that originates from the presence of these large granules. Consequently, the motion of yolk granules reflects the evolution of the effective viscosity of the surrounding medium during heat-induced gelation in the temperature range studied here. Upon heating from room temperature, a gradual decrease in τ is observed during the heat ramp, which follows a power law $\sim (t'_w)^{-0.3}$. We anticipate that this behavior arises from enhanced kinetic energy of the yolk granules coupled with the temperature-dependent reduction in the viscosity of the aqueous phase.

Once the sample reaches the set temperature [indicated by vertical markers near the x-axis in Figs. 7(a)–7(d)], a transition to regime B is observed, marking the onset of thermal equilibration. In regime B, the relaxation time τ exhibits a power-law increase with waiting time, indicating a progressive reduction in microscopic mobility as structural changes develop in the system. Egg yolk plasma proteins are known to undergo denaturation at temperatures above 60 °C.[70] As thermal denaturation proceeds, proteins expose reactive functional groups that enhance intermolecular interactions, including the formation of disulfide bonds, and promote protein aggregation.[71,72,75] The gradual buildup of these aggregates provides a physical basis for the observed continuous slowing down

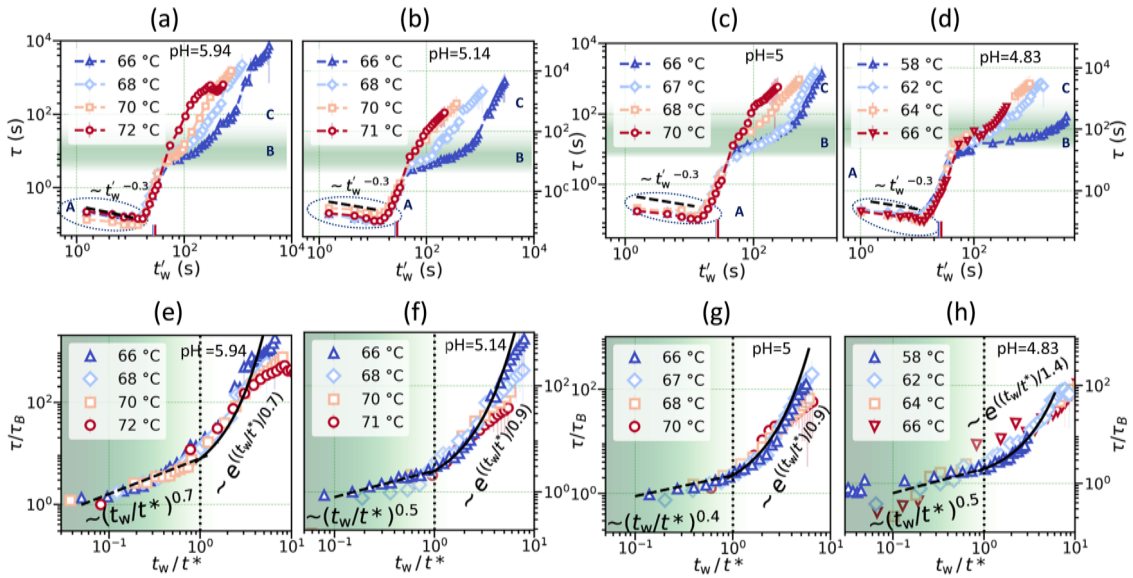

FIG. 7. Relaxation time of (a) yolk, (b) y600, (c) y800, and (d) y1000 at several temperatures, as indicated in the legends. All τ values are extracted at $q = 0.0055$ nm^{-1}. Short vertical ticks along the horizontal axis denote $t_{heating}$ (time taken to reach the set temperature from 22 °C). The color of these lines matches that of the data points at the same temperature. Regime A is highlighted by a dotted circle, while regime B is indicated by a green-shaded region. Relaxation time (τ), normalized by the equilibrium relaxation time at the set temperature (τ_B—the relaxation time at the beginning of regime B), as a function of normalized isothermal waiting time (t_w/t^*) for (e) yolk, (f) y600, (g) y800, and (h) y1000.

of the dynamics in regime B. Following regime B, a clear dynamical transition from power-law behavior to an exponential slowdown is observed (regime C), with the transition time decreasing as the temperature increases. Such an exponential arrest of the dynamics is a well-established signature of sol–gel transitions in protein, polymer, and colloidal systems.[8,76,77] Protein denaturation-driven gelation is expected to manifest as a rapid increase in the relaxation time by several orders of magnitude, reflecting the development of a mechanically arrested network. Since the sol–gel transition is characterized by a strong increase in viscosity,[78] and the relaxation time τ is directly linked to the local viscosity probed by XPCS, the pronounced slowdown observed in regime C provides clear dynamical evidence for the formation of a yolk gel network.

The relaxation times, normalized by the equilibrium value from regime B, are plotted as a function of the isothermal waiting time normalized by the sol–gel transition time t^* (from kinetic measurements), resulting in a master curve, as shown in Figs. 7(e)–7(h). This normalization mitigates sample-to-sample variations in τ arising from the intrinsic heterogeneity of the sample. Complementary viscometry measurements on egg yolk show good agreement between the sol–gel transition times estimated from XPCS and from viscometry.[6] The green-colored region on the left side of the plot indicates regime B. This master curve highlights the presence of TTS in yolk gelation dynamics, showing that all samples follow a common gelation mechanism influenced by temperature-dependent reaction rates. Notably, Fig. 5 reveals two power-law regimes in the structural evolution, separated by the gelation time t^*, while Figs. 7(e)–7(h) show that the relaxation time exhibits a distinct crossover at the same t^*, transitioning from a power-law to an exponential slowdown. Together, these master curves provide complementary insight, demonstrating that a full understanding of thermal gelation at acidic pH requires coupling structural information with dynamical signatures.

Figure 8(a) presents the Arrhenius plot for t^*, where the observed values of pure yolk align closely with those reported in our earlier study.[6] To gain deeper insight, we fit the t^* values using the Arrhenius equation,[79,80] allowing quantification of the temperature dependence:

$$t^* = A\, e^{\left(\frac{E_a}{RT}\right)}, \tag{4}$$

$$\ln\,(t^*) = \frac{E_a}{RT} + \ln\,(A), \tag{5}$$

where E_a is the activation energy, R is the universal gas constant, and T is the temperature in Kelvin. The term $1/A$, often referred to as the frequency factor or attempt frequency, reflects the frequency of collisions between reactant molecules. Here, the Arrhenius law is an approximate description for this complex system.

Lowering the pH by adding citric acid does not significantly affect the activation energy of egg yolk gelation, consistent with findings from other protein systems.[15,81] The fitted activation energy remains approximately constant at a value of 450 ± 20 kJ/mol (≈108 kcal/mol or 4.7 eV).

Interestingly, as shown in Fig. 8(b), the sol–gel transition time at a fixed temperature (T = 66 °C) decreases with decreasing pH (i.e., increasing citric acid concentration). This indicates that acidification significantly promotes the gelation process, likely by modulating the interactions driving protein denaturation and aggregation. Notably, while the overall kinetics are accelerated, the underlying gelation mechanism remains unchanged—evidenced by the collapse of relaxation time data onto a master curve when time is normalized by the sol–gel transition point [Figs. 7(e)–7(h)].

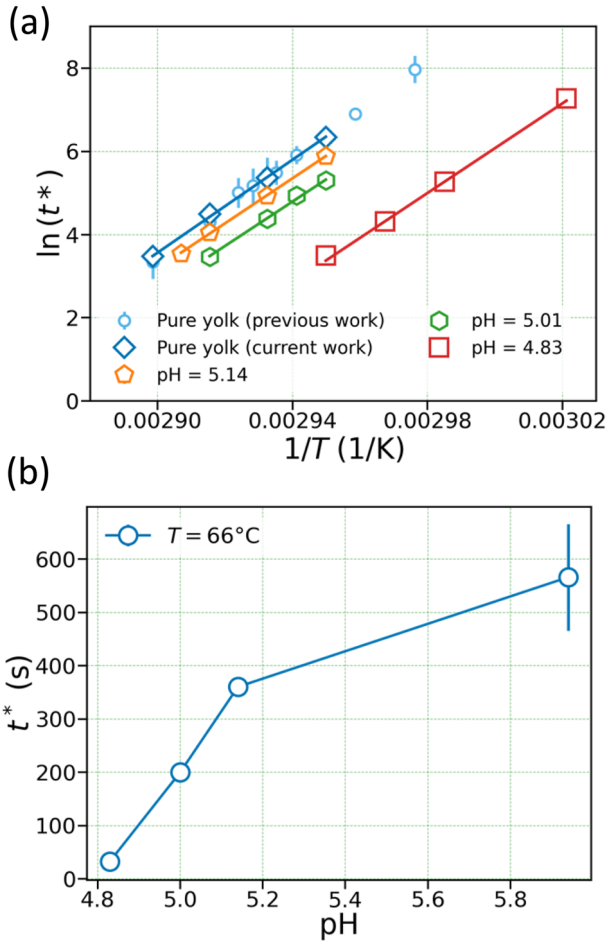

FIG. 8. (a) Arrhenius plot illustrating the temperature dependence of t^* at various acidic pH levels. Circular markers represent data from our previous study[6] for pure egg yolk. The solid lines show fits using Eq. (5). The solid lines represent fits using Eq. (5). The extracted activation energy from the fits is 450 ± 20 kJ/mol. (b) Variation of t^* with acidic pH values at T = 66 °C.

Our results show that acidified egg yolks gel faster during heating because low pH promotes partial denaturation, reduces electrostatic repulsion, and enhances aggregation of yolk proteins. While the activation energy E_a remains constant, the prefactor A decreases systematically with decreasing pH [indicated by the shift of curves in Fig. 8(a)], corresponding to a shorter gelation time [Fig. 8(b)] without a change in the energy barrier. This points to a separation of roles: lowering the pH primarily increases the probability of productive encounters—most plausibly by reducing electrostatic repulsion and thereby enhancing the lifetime of protein–protein contacts—whereas the subsequent bond-formation

or restructuring step that locks these contacts into a gel network is governed by an activated process whose energy barrier is overall pH-independent.

By systematically comparing the effects of ionic strength[7] and pH (present study) on thermal gelation within a unified experimental framework,[6] we show that the characteristic activation energy associated with egg-yolk gelation remains similar across different biochemical environments, even though the scaling laws underlying kinetics and dynamics differ substantially. This comparative approach indicates that variations in ionic strength or pH primarily influence the efficiency and likelihood of productive protein–protein encounters, while the energetic barrier associated with the formation of a gel network appears to be largely preserved. From a food-processing perspective, this finding is particularly relevant, as pH and salt concentration are routinely adjusted during the formulation, preservation, and thermal processing of egg-based products to control texture, stability, and functionality. Understanding how these parameters modulate gelation kinetics without fundamentally altering the underlying energy landscape provides a physicochemical basis for optimizing processing conditions while maintaining consistent product quality.

Next, we compare our findings with other protein systems. Previous studies have reported that the activation energy of gelation for whey proteins[81] and soy proteins[15] remains unaffected by changes in pH, which aligns with our observations in acidified egg yolks. Similarly, the activation energy was found to be independent of ionic strength variations in both soy protein systems[82] and egg yolk.[7] This suggests that modifying pH or ionic strength may influence gelation behavior (gel strength or onset time) but not the fundamental energy barrier (E_a) needed for gelation to occur, at least for some protein systems.

IV. CONCLUSION

In summary, we investigated the changes in the structural and dynamical evolution of hen egg yolk during heat-induced gelation upon acidification using low-dose USAXS-XPCS. Acid-induced lowering of pH led to partial denaturation of yolk proteins, while LDLs remained morphologically stable across the examined pH range. The rates of denaturation, aggregation, and gelation processes were strongly accelerated by decreasing pH. Despite these kinetic enhancements, the observation of time–temperature superposition across temperatures at each pH indicates that the mechanism is the same across temperatures for a given pH, with pH primarily shifting the intrinsic timescale of the gelation process. The sol–gel transition times derived from both structural and dynamical observables can be described by an effective Arrhenius law. While the extracted activation energy, E_a, remains largely unaffected by pH variation, the prefactor A decreases systematically with decreasing pH, corresponding to a shorter gelation time without altering the fundamental energy barrier. This indicates that acidification modulates gelation primarily by increasing the probability of productive encounters—most plausibly by reducing electrostatic repulsion and thereby enhancing the lifetime of protein–protein contacts—whereas the subsequent bond-formation or restructuring step that locks these contacts into a gel network is governed by an activated process whose energy landscape remains essentially pH-independent.

SUPPLEMENTARY MATERIAL

Calibration of the Linkam heating cell; estimation of citric acid weight percent in acidified yolk mixtures; structural features of egg yolk components at room temperature in pure yolk; $I(q)$ of yolk at different pH; scattering invariant of acidified yolks; wave-vector-dependent τ and γ of all samples at room temperature; comparison of the acidity of y600 to kitchen values; and discussion of the X-ray beam influence on the structure and dynamics of egg yolk.

ACKNOWLEDGMENTS

We acknowledge DESY (Hamburg, Germany), a member of the Helmholtz Association HGF, for the provision of experimental facilities. Parts of this research were carried out at the beamline P10 during in-house beamtimes. The authors also acknowledge the support of DFG (No. NFDI 40/1), BMBF (Nos. 05K19PS1, 05K20PSA, and 05K22PS1), and NFDI for this work. M.P. thanks the DELTA machine group for providing synchrotron radiation for sample characterization. This work was supported through the Maxwell computational resources operated at Deutsches Elektronen-Synchrotron DESY, Hamburg, Germany.

AUTHOR DECLARATIONS

Conflict of Interest

The authors have no conflicts to disclose.

Author Contributions

Nimmi Das Anthuparambil: Conceptualization (lead); Data curation (lead); Formal analysis (lead); Investigation (lead); Validation (lead); Visualization (lead); Writing – original draft (lead); Writing – review & editing (lead). **Sonja Timmermann**: Data curation (supporting); Investigation (supporting). **Michelle Dargasz**: Investigation (supporting); Writing – review & editing (supporting). **Sebastian Retzbach**: Investigation (supporting); Writing – review & editing (supporting). **Maximilian D. Senft**: Investigation (supporting). **Fajun Zhang**: Investigation (supporting); Writing – review & editing (supporting). **Michael Paulus**: Investigation (supporting); Resources (supporting); Writing – review & editing (supporting). **Fabian Westermeier**: Resources (equal); Software (equal); Writing – review & editing (supporting). **Michael Sprung**: Resources (equal); Software (equal). **Frank Schreiber**: Conceptualization (supporting); Funding acquisition (equal); Writing – review & editing (supporting). **Christian Gutt**: Conceptualization (equal); Funding acquisition (lead); Writing – review & editing (supporting).

DATA AVAILABILITY

Raw data were generated at PETRA III, Hamburg, Germany. Derived data supporting the findings of this study are available from the corresponding author upon reasonable request.

REFERENCES

[1] R. Mezzenga, P. Schurtenberger, A. Burbidge, and M. Michel, "Understanding foods as soft materials," Nat. Mater. **4**, 729–740 (2005).

[2]S. Assenza and R. Mezzenga, "Soft condensed matter physics of foods and macronutrients," Nat. Rev. Phys. **1**, 551–566 (2019).
[3]B. Caviglia, S. Timr, M. Guiral, M.-T. Giudici-Orticoni, T. Seydel, C. Beck, J. Peters, F. Sterpone, and A. Paciaroni, "Cytoplasmic fluidity and the cold life: Proteome stability is decoupled from viability in psychrophiles," Nat. Commun. **16**, 10345 (2025).
[4]M. Grimaldo, F. Roosen-Runge, M. Hennig, F. Zanini, F. Zhang, N. Jalarvo, M. Zamponi, F. Schreiber, and T. Seydel, "Hierarchical molecular dynamics of bovine serum albumin in concentrated aqueous solution below and above thermal denaturation," Phys. Chem. Chem. Phys. **17**, 4645–4655 (2015).
[5]Y. Zhao, F. Feng, Y. Yang, C. Xiong, M. Xu, and Y. Tu, "Gelation behavior of egg yolk under physical and chemical induction: A review," Food Chem. **355**, 129569 (2021).
[6]N. D. Anthuparambil, A. Girelli, S. Timmermann, M. Kowalski, M. S. Akhundzadeh, S. Retzbach, M. D. Senft, M. Dargasz, D. Gutmüller, A. Hiremath *et al.*, "Exploring non-equilibrium processes and spatio-temporal scaling laws in heated egg yolk using coherent X-rays," Nat. Commun. **14**, 5580 (2023).
[7]N. D. Anthuparambil, S. Timmermann, M. Dargasz, S. Retzbach, M. D. Senft, N. Begam, A. Ragulskaya, M. Paulus, F. Zhang, F. Westermeier *et al.*, "Salt induced slowdown of kinetics and dynamics during thermal gelation of egg-yolk," J. Chem. Phys. **161**, 055102 (2024).
[8]N. Begam *et al.*, "Kinetics of network formation and heterogeneous dynamics of an egg white gel revealed by coherent X-ray scattering," Phys. Rev. Lett. **126**, 098001 (2021).
[9]N. Begam, S. Timmermann, A. Ragulskaya, A. Girelli, M. D. Senft, S. Retzbach, N. D. Anthuparambil, M. S. Akhundzadeh, M. Kowalski, M. Reiser *et al.*, "Effects of temperature and ionic strength on the microscopic structure and dynamics of egg white gels," J. Chem. Phys. **158**, 074903 (2023).
[10]N. Chen, M. Zhao, C. Chassenieux, and T. Nicolai, "The effect of adding NaCl on thermal aggregation and gelation of soy protein isolate," Food Hydrocolloids **70**, 88–95 (2017).
[11]F. Roosen-Runge, B. S. Heck, F. Zhang, O. Kohlbacher, and F. Schreiber, "Interplay of pH and binding of multivalent metal ions: Charge inversion and reentrant condensation in protein solutions," J. Phys. Chem. B **117**, 5777–5787 (2013).
[12]M. Sadeghi, A. Madadlou, A. Khosrowshahi, and M. Mohammadifar, "Acid-induced gelation behavior of casein/whey protein solutions assessed by oscillatory rheology," J. Food Sci. Technol. **51**, 2113–2119 (2014).
[13]J. M. Aguilar, F. Cordobés, C. Bengoechea, and A. Guerrero, "Heat-induced gelation of egg yolk as a function of pH. Does the type of acid make any difference?," Food Hydrocolloids **87**, 142–148 (2019).
[14]J. M. Aguilar, M. Felix, Y. López-González, F. Cordobés, and A. Guerrero, "Acidic and heat processing of egg yolk dispersions," Processes **9**, 1842 (2021).
[15]N. Chen, M. Zhao, F. Niepceron, T. Nicolai, and C. Chassenieux, "The effect of the pH on thermal aggregation and gelation of soy proteins," Food Hydrocolloids **66**, 27–36 (2017).
[16]Y. Lian, Y. Li, R. Lv, L. Wang, and W. Xiong, "The mechanism of alkali-induced rice protein gel formation: Effect of alkali concentration and temperature," Food Hydrocolloids **147**, 109335 (2024).
[17]X. Gao, Y. Yao, N. Wu, M. Xu, Y. Zhao, and Y. Tu, "The sol-gel-sol transformation behavior of egg white proteins induced by alkali," Int. J. Biol. Macromol. **155**, 588–597 (2020).
[18]N. Yuno-Ohta, T. Higasa, E. Tatsumi, H. Sakurai, R. Asano, and M. Hirose, "Formation of fatty acid salt-induced gel of ovalbumin and the mechanism for gelation," J. Agric. Food Chem. **46**, 4518–4523 (1998).
[19]N. Nio, M. Motoki, and K. Takinami, "Gelation mechanism of protein solution by transglutaminase," Agric. Biol. Chem. **50**, 851–855 (1986).
[20]J. F. Zayas, "Gelling properties of proteins," in *Functionality of Proteins in Food* (Springer Berlin Heidelberg, 1997), pp. 310–366.
[21]R. Huopalahti, M. Anton, R. López-Fandiño, and R. Schade, *Bioactive Egg Compounds* (Springer, Berlin, 2007), Vol. 5.
[22]T. Nicolai, "Gelation of food protein-protein mixtures," Adv. Colloid Interface Sci. **270**, 147–164 (2019).
[23]K. B. Djagny, Z. Wang, and S. Xu, "Gelatin: A valuable protein for food and pharmaceutical industries," Crit. Rev. Food Sci. Nutr. **41**, 481–492 (2001).
[24]M. L. Floren, S. Spilimbergo, A. Motta, and C. Migliaresi, "Carbon dioxide induced silk protein gelation for biomedical applications," Biomacromolecules **13**, 2060–2072 (2012).
[25]A. Rodil *et al.*, "Gels prepared from egg yolk and its fractions for tissue engineering," Biotechnol. Prog. **32**, 1577–1583 (2016).
[26]Y. Mine, *Egg Bioscience and Biotechnology* (John Wiley & Sons, 2008).
[27]J. Li, J. Zhai, L. Gu, Y. Su, L. Gong, Y. Yang, and C. Chang, "Hen egg yolk in food industry—A review of emerging functional modifications and applications," Trends Food Sci. Technol. **115**, 12–21 (2021).
[28]A. Laca, B. Paredes, M. Rendueles, and M. Díaz, "Egg yolk granules: Separation, characteristics and applications in food industry," LWT-Food Sci. Technol. **59**, 1–5 (2014).
[29]L. Gu, Y. Liu, W. Zhang, J. Li, C. Chang, Y. Su, and Y. Yang, "Novel extraction technologies and potential applications of egg yolk proteins," Food Sci. Biotechnol. **32**, 121–133 (2023).
[30]M. Anton, "Egg yolk: Structures, functionalities and processes," J. Sci. Food Agric. **93**, 2871–2880 (2013).
[31]S.-C. Yang and R. E. Baldwin, "Functional properties of eggs in foods," in *Egg Science and Technology* (CRC Press, 2017), pp. 405–463.
[32]N. M. Anderson, J. W. Larkin, M. B. Cole, G. E. Skinner, R. C. Whiting, L. G. M. Gorris, A. Rodriguez, R. Buchanan, C. M. Stewart, J. H. Hanlin *et al.*, "Food safety objective approach for controlling *Clostridium botulinum* growth and toxin production in commercially sterile foods," J. Food Prot. **74**, 1956–1989 (2011).
[33]L. Nielsen and S. Knøchel, "Inactivation of salmonella strains in acidified broth and raw egg yolk as a function of pH and acid type," Food Microbiol. **92**, 103574 (2020).
[34]S. D. Arntfield, E. D. Murray, and M. A. H. Ismond, "Influence of salts on the microstructural and rheological properties of heat-induced protein networks from ovalbumin and vicilin," J. Agric. Food Chem. **38**, 1335–1343 (1990).
[35]T. Kaewmanee, S. Benjakul, W. Visessanguan, and C. Gamonpilas, "Effect of sodium chloride and osmotic dehydration on viscoelastic properties and thermal-induced transitions of duck egg yolk," Food Bioprocess Technol. **6**, 367–376 (2013).
[36]M. Grimaldo, F. Roosen-Runge, F. Zhang, F. Schreiber, and T. Seydel, "Dynamics of proteins in solution," Q. Rev. Biophys. **52**, e7 (2019).
[37]S. Timmermann, N. D. Anthuparambil, A. Girelli, N. Begam, M. Kowalski, S. Retzbach, M. D. Senft, M. S. Akhundzadeh, H.-F. Poggemann, M. Moron *et al.*, "X-ray driven and intrinsic dynamics in protein gels," Sci. Rep. **13**, 11048 (2023).
[38]M. Moron *et al.*, "Gelation dynamics upon pressure-induced liquid–liquid phase separation in a water–lysozyme solution," J. Phys. Chem. B **126**, 4160–4167 (2022).
[39]A. Girelli *et al.*, "Microscopic dynamics of liquid-liquid phase separation and domain coarsening in a protein solution revealed by X-ray photon correlation spectroscopy," Phys. Rev. Lett. **126**, 138004 (2021).
[40]A. Ragulskaya, N. Begam, A. Girelli, H. Rahmann, M. Reiser, F. Westermeier, M. Sprung, F. Zhang, C. Gutt, and F. Schreiber, "Interplay between kinetics and dynamics of liquid–liquid phase separation in a protein solution revealed by coherent X-ray spectroscopy," J. Phys. Chem. Lett. **12**, 7085–7090 (2021).
[41]N. D. Anthuparambil, M. Dargasz, S. Timmermann, A. Girelli, S. Retzbach, J. Möller, W. Jo, A. M. Raza, A. Leonau, J. Wrigley *et al.*, "Lipoprotein diffusion in dense yolk plasma is governed by softness, hydrodynamics, and caging: Insights from MHz-XPCS," Proc. Natl. Acad. Sci. U. S. A. **123**, e2519681123 (2026).
[42]N. Das, N. Begam, M. Ibrahim, S. Chandran, V. Padmanabhan, M. Sprung, and J. K. Basu, "Viscosity and fragility of confined polymer nanocomposites: A tale of two interfaces," Nanoscale **11**, 8546–8553 (2019).
[43]N. Begam, N. Das, S. Chandran, M. Ibrahim, V. Padmanabhan, M. Sprung, and J. Basu, "Nanoparticle–polymer interfacial layer properties tune fragility and dynamic heterogeneity of athermal polymer nanocomposite films," Soft Matter **14**, 8853–8859 (2018).
[44]N. Das A, N. Begam, S. Chandran, A. Swain, M. Sprung, and J. K. Basu, "Thermal stability and dynamics of soft nanoparticle membranes: Role of entropy, enthalpy and membrane compressibility," Soft Matter **16**, 1117–1124 (2020).
[45]A. Jain, F. Schulz, I. Lokteva, L. Frenzel, G. Grübel, and F. Lehmkühler, "Anisotropic and heterogeneous dynamics in an aging colloidal gel," Soft Matter **16**, 2864–2872 (2020).

[46]B. Ruta, G. Baldi, Y. Chushkin, B. Rufflé, L. Cristofolini, A. Fontana, M. Zanatta, and F. Nazzani, "Revealing the fast atomic motion of network glasses," Nat. Commun. **5**, 3939 (2014).
[47]Q. Zhang, E. M. Dufresne, and A. R. Sandy, "Dynamics in hard condensed matter probed by X-ray photon correlation spectroscopy: Present and beyond," Curr. Opin. Solid State Mater. Sci. **22**, 202–212 (2018).
[48]J. Song, Q. Zhang, F. de Quesada, M. H. Rizvi, J. B. Tracy, J. Ilavsky, S. Narayanan, E. Del Gado, R. L. Leheny, N. Holten-Andersen, and G. H. McKinley, "Microscopic dynamics underlying the stress relaxation of arrested soft materials," Proc. Natl. Acad. Sci. U. S. A. **119**, e2201566119 (2022).
[49]W. J. Stadelman and O. J. Cotterill, *Egg Science and Technology*, 4th ed. (CRC Press, Boca Raton, FL, 1995).
[50]C. Chang, W. Powrie, and O. Fennema, "Microstructure of egg yolk," J. Food Sci. **42**, 1193–1200 (1977).
[51]R. Bellairs, "The structure of the yolk of the hen's egg as studied by electron microscopy: I. The yolk of the unincubated egg," J. Cell Biol. **11**, 207–225 (1961).
[52]L. Xu, Y. Zhao, M. Xu, Y. Yao, N. Wu, H. Du, and Y. Tu, "Changes in physicochemical properties, microstructure, protein structures and intermolecular force of egg yolk, plasma and granule gels during salting," Food Chem. **275**, 600–609 (2019).
[53]M. Anton, M. L. Denmat, and G. Gandemer, "Thermostability of hen egg yolk granules: Contribution of native structure of granules," J. Food Sci. **65**, 581–584 (2000).
[54]T. Strixner, J. Sterr, U. Kulozik, and R. Gebhardt, "Structural study on hen-egg yolk high density lipoprotein (HDL) granules," Food Biophys. **9**, 314–321 (2014).
[55]M. Reiser *et al.*, "Resolving molecular diffusion and aggregation of antibody proteins with megahertz X-ray free-electron laser pulses," Nat. Commun. **13**, 5528 (2022).
[56]G. Pintori, G. Baldi, B. Ruta, and G. Monaco, "Relaxation dynamics induced in glasses by absorption of hard X-ray photons," Phys. Rev. B **99**, 224206 (2019).
[57]Y. Chushkin *et al.*, "Probing cage relaxation in concentrated protein solutions by X-ray photon correlation spectroscopy," Phys. Rev. Lett. **129**, 238001 (2022).
[58]M. Reiser and R. Rosca, https://github.com/reiserm/Xana.
[59]O. Bikondoa, "On the use of two-time correlation functions for X-ray photon correlation spectroscopy data analysis," J. Appl. Crystallogr. **50**, 357–368 (2017).
[60]A. Madsen, R. L. Leheny, H. Guo, M. Sprung, and O. Czakkel, "Beyond simple exponential correlation functions and equilibrium dynamics in X-ray photon correlation spectroscopy," New J. Phys. **12**, 055001 (2010).
[61]O. G. Shpyrko, "X-ray photon correlation spectroscopy," J. Synchrotron Radiat. **21**, 1057–1064 (2014).
[62]A. Ragulskaya, V. Starostin, F. Zhang, C. Gutt, and F. Schreiber, "On the analysis of two-time correlation functions: Equilibrium versus non-equilibrium systems," J. Appl. Crystallogr. **57**, 1098–1106 (2024).
[63]F. Perakis and C. Gutt, "Towards molecular movies with X-ray photon correlation spectroscopy," Phys. Chem. Chem. Phys. **22**, 19443–19453 (2020).
[64]G. Williams and D. C. Watts, "Non-symmetrical dielectric relaxation behaviour arising from a simple empirical decay function," Trans. Faraday Soc. **66**, 80–85 (1970).
[65]L. Cipelletti, L. Ramos, S. Manley, E. Pitard, D. A. Weitz, E. E. Pashkovski, and M. Johansson, "Universal non-diffusive slow dynamics in aging soft matter," Faraday Discuss. **123**, 237–251 (2003).
[66]A. Fluerasu, A. Moussaïd, A. Madsen, and A. Schofield, "Slow dynamics and aging in colloidal gels studied by x-ray photon correlation spectroscopy," Phys. Rev. E **76**, 010401 (2007).
[67]B. Chung, S. Ramakrishnan, R. Bandyopadhyay, D. Liang, C. F. Zukoski, J. L. Harden, and R. L. Leheny, "Microscopic dynamics of recovery in sheared depletion gels," Phys. Rev. Lett. **96**, 228301 (2006).
[68]B. Ruta, G. Baldi, G. Monaco, and Y. Chushkin, "Compressed correlation functions and fast aging dynamics in metallic glasses," J. Chem. Phys. **138**, 054508 (2013).
[69]P. Baur, G. Nägele, and R. Klein, "Nonexponential relaxation of density fluctuations in charge-stabilized colloids," Phys. Rev. E **53**, 6224–6237 (1996).
[70]D. Dixon and O. Cotterill, "Electrophoretic and chromatographic changes in egg yolk proteins due to heat," J. Food Sci. **46**, 981–983 (1981).
[71]T. Nguyen and R. Burley, "Studies on the apoproteins of the major lipoprotein of the yolk of hen's eggs. V. Protein sulfhydryl groups: Accessibility in the lipoprotein and the effect of temperature," Aust. J. Biol. Sci. **37**, 7–16 (1984).
[72]V. Kiosseoglou and A. Paraskevopoulou, "Molecular interactions in gels prepared with egg yolk and its fractions," Food Hydrocolloids **19**, 527–532 (2005).
[73]S. Navidghasemizad, F. Temelli, and J. Wu, "Phase separation behavior of egg yolk suspensions after anionic polysaccharides addition," Carbohydr. Polym. **117**, 297–303 (2015).
[74]M. Bautista Villarreal, C. T. Gallardo Rivera, E. García Márquez, J. Rodríguez Rodríguez, M. A. Núñez González, A. Chávez Montes, and J. G. Báez González, "Comparative reduction of egg yolk cholesterol using anionic chelating agents," Molecules **23**, 3204 (2018).
[75]A. H. Clark, G. M. Kavanagh, and S. B. Ross-Murphy, "Globular protein gelation—Theory and experiment," Food Hydrocolloids **15**, 383–400 (2001).
[76]D. Bahadur *et al.*, "Evolution of structure and dynamics of thermo-reversible nanoparticle gels—A combined XPCS and rheology study," J. Chem. Phys. **151**, 104902 (2019).
[77]L. Frenzel, M. Dartsch, G. M. Balaguer, F. Westermeier, G. Grübel, and F. Lehmkühler, "Glass-liquid and glass-gel transitions of soft-shell particles," Phys. Rev. E **104**, L012602 (2021).
[78]C. Le Bon, T. Nicolai, and D. Durand, "Kinetics of aggregation and gelation of globular proteins after heat-induced denaturation," Macromolecules **32**, 6120–6127 (1999).
[79]M. Lu, D. L. Gantz, H. Herscovitz, and O. Gursky, "Kinetic analysis of thermal stability of human low density lipoproteins: A model for LDL fusion in atherogenesis," J. Lipid Res. **53**, 2175–2185 (2012).
[80]C. Vega and R. Mercadé-Prieto, "Culinary biophysics: On the nature of the 6X° C egg," Food Biophys. **6**, 152–159 (2011).
[81]A. Kharlamova, C. Chassenieux, and T. Nicolai, "Acid-induced gelation of whey protein aggregates: Kinetics, gel structure and rheological properties," Food Hydrocolloids **81**, 263–272 (2018).
[82]N. Chen, C. Chassenieux, and T. Nicolai, "Kinetics of NaCl induced gelation of soy protein aggregates: Effects of temperature, aggregate size, and protein concentration," Food Hydrocolloids **77**, 66–74 (2018).